Experimental Identification of Electric Dipoles Induced by Magnetic Monopoles in $Tb_2Ti_2O_7$

Feng Jin,[1,2] Changle Liu,[3] Yanfen Chang,[1] Anmin Zhang,[4] Yimeng Wang,[1,2] Weiwei Liu,[1,2] Xiaoqun Wang,[5] Young Sun,[1] Gang Chen,[6,3] Xuefeng Sun,[7] and Qingming Zhang[4,1,*]

[1]*Beijing National Laboratory for Condensed Matter Physics, Institute of Physics, Chinese Academy of Sciences, Beijing 100190, China*
[2]*Department of Physics, Renmin University of China, Beijing 100872, China*
[3]*State Key Laboratory of Surface Physics and Department of Physics, Fudan University, Shanghai 200433, China*
[4]*School of Physical Science and Technology, Lanzhou University, Lanzhou 730000, China*
[5]*Key Laboratory of Artificial Structures and Quantum Control of MOE, Shenyang National Laboratory for Materials Science, School of Physics and Astronomy, Tsung-Dao Lee Institute, Shanghai Jiao Tong University, Shanghai 200240, China*
[6]*Department of Physics and Center of Theoretical and Computational Physics, The University of Hong Kong, Pokfulam Road, Hong Kong, China*
[7]*Hefei National Laboratory for Physical Sciences at Microscale, University of Science and Technology of China, Hefei, Anhui 230026, China*

(Received 29 July 2019; accepted 7 February 2020; published 27 February 2020)

The fundamental principles of electrodynamics allow an electron carrying both electric monopole (charge) and magnetic dipole (spin) but prohibit its magnetic counterpart. Recently, it was predicted that the magnetic "monopoles" carrying emergent magnetic charges in spin ice systems can induce electric dipoles. The inspiring prediction offers a novel way to study magnetic monopole excitations and magnetoelectric coupling. However, no clear example has been identified up to now. Here, we report the experimental evidence for electric dipoles induced by magnetic monopoles in spin frustrated $Tb_2Ti_2O_7$. The magnetic field applied to pyrochlore $Tb_2Ti_2O_7$ along the [111] direction, brings out a "3-in-1-out" magnetic monopole configuration, and then induces a subtle structural phase transition at $H_c \sim 2.3$ T. The transition is made evident by the nonlinear phonon splitting under magnetic fields and the anomalous crystal-field excitations of Tb^{3+} ions. The observations consistently point to the displacement of the oxygen O″ anions along the [111] axis which gives rise to the formation of electric dipoles. The finding demonstrates that the scenario of magnetic monopole having both magnetic charge and electric dipole is realized in $Tb_2Ti_2O_7$ and sheds light into the coupling between electricity and magnetism of magnetic monopoles in spin frustrated systems.

DOI: 10.1103/PhysRevLett.124.087601

The interplay of electricity and magnetism is always a central topic in fundamental physics. In recent decades, the topic has received renewed attention in many exciting fields such as multiferroics, magnetoelectrics, and spintronics [1,2]. The coexistence of various degrees of freedom (lattice, charge, and spin) and their mutual entanglement, output a large variety of unusual effects and responses [3]. These systems represent excellent platforms for quantum control and engineering in both fundamental research and practical applications.

Recently, Khomskii *et al.* proposed a fascinating scenario that in spin ice compounds the magnetic monopoles should be accompanied with electric dipoles [4,5]. The attachment of electric dipoles on magnetic monopoles enables us to study and control such exotic magnetic monopoles by means of electric fields [6], and offers a novel way to develop potential applications in quantum computation. In spin ice systems, magnetic monopoles are topological defects of spin ice textures where within one tetrahedra the 2-in-2-out ice rule is violated [7,8]. Spin ice realistic systems can be realized in rare-earth pyrochlore and spinel compounds. Besides, many of these materials exhibit large magnetoelectric coupling that is also regarded as one of the essential ingredients to realize multiferroicity [9,10].

The effort of looking for the ideal candidate demonstrating both magnetic monopole and electric dipoles, is thus focused on the pyrochlore family with strong magnetoelectric coupling. Recently, it was theoretically pointed out that one of the family members, $Tb_2Ti_2O_7$, is perhaps a good candidate to realize such a scenario in its magnetic monopole structures [11]. Despite the complications of low-lying crystal-field levels [12–14] in this material, it shows unfreezing behaviors down to 50 mK [15] and the pinch point correlations at low temperatures [16–19], suggesting that this material may be in a quantum spin ice state. Moreover, this material hosts giant spin-lattice coupling [20–24]. Thus, it is believed that $Tb_2Ti_2O_7$ represents a promising candidate to realize Khomskii's proposal. While the field-induced magnetic monopole-antimonopole structure has been reported by

previous neutron experiments [25,26], to the best of our knowledge, the induced electric dipoles and their coupling with magnetic monopoles have not been clearly identified on the experimental side.

In this Letter, we employed magneto-Raman and magnetodielectric technique to search for electric dipoles induced by magnetic monopoles in the pyrochlore $Tb_2Ti_2O_7$. The alternating magnetic monopole-antimonopole structure is stabilized by magnetic fields along the [111] axis [25]. Meanwhile, the field-induced electric dipoles are manifested by the pronounced rise of dielectric permittivity and the subtle structural changes captured by our Raman measurements. The application of magnetic fields results in the unusual nonlinear phonon splitting, the anomalous splitting of crystal-field excitations (CFEs) and the emergence of new CFEs. The observations can be consistently and well explained in term of the shift of the oxygen (O″) along [111] axis that gives rise to electric dipoles. The findings demonstrate that electric dipoles induced by magnetic monopoles and the strong coupling between them are unambiguously identified in $Tb_2Ti_2O_7$. This opens new possibilities to control magnetic monopoles with electric fields.

The high quality of the $Tb_2Ti_2O_7$ single crystal was grown by the floating-zone technique [27] and has been characterized before measurements [28]. Confocal micro-Raman measurements were performed with a backscattering configuration using a Jobin Yvon T64000 system and a 532-nm diode-pumped solid-state laser. The laser power was kept at a level of 500 μW to avoid overheating. Magnetic fields were generated up to 9 T using a superconducting magnet, and the direction of the magnetic field was along the [111] axis with an accuracy of $\pm 2°$. The dielectric measurements were carried out in a Cryogen-Free Superconducting Magnet System (Oxford Instruments, TeslatronPT). An Agilent 4980A LCR meter was used to measure the dielectric permittivity with the frequency $f = 1$ MHz.

The Raman spectra taken at 10 K and 0 T are shown in Fig. 1(a), in which three strong phonon modes appear at ~289 (F_{2g}), 320 (E_g), and 511 (A_{1g}) cm^{-1}. According to previous reports [29,30], the F_{2g} mode is assigned as the combined vibration of O′ (48f) and O″ (8a) anions while the A_{1g} and E_g modes are solely due to the vibration of O′ anions. With the application of magnetic field along [111] axis, the A_{1g} mode is nearly unchanged but the F_{2g} mode shows a clear splitting and eventually evolves into two well-resolved modes ($P1$ and $P2$) at 9 T [Fig. 1(b)].

The photoluminescence origin of $P1$ or $P2$ can be easily excluded since they remain unchanged under different excitation sources [Fig. 1(a)]. The magnetic origin is also unlikely because of the very small magnetic exchange energy in $Tb_2Ti_2O_7$ ($\Theta_{CW} \approx -19$ K) [15]. And the CFE origin is incompatible with the following characteristics of the two modes [28]: (1) the $P1$ and $P2$ intensities are almost

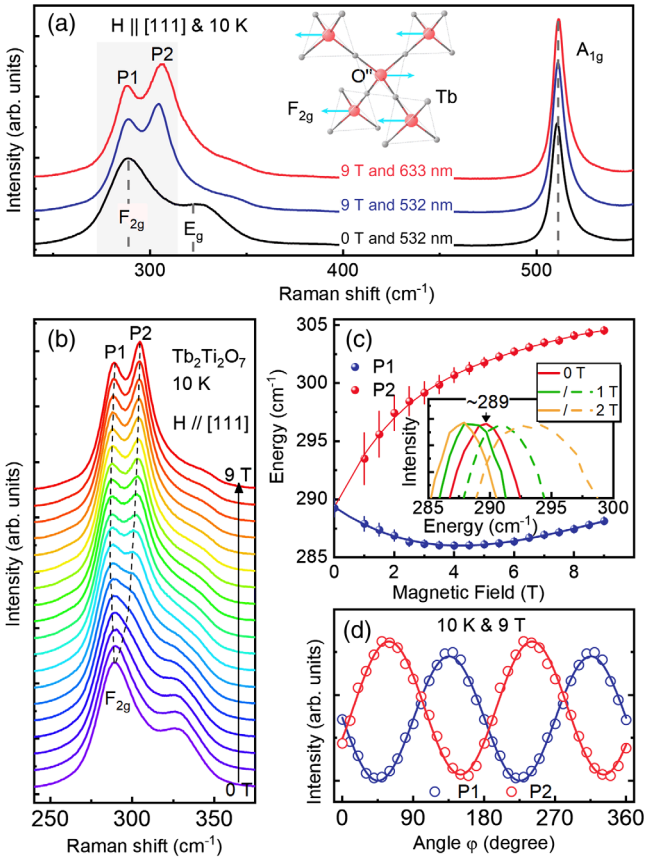

FIG. 1. [111]-field induced splitting of the F_{2g} phonon. (a) Raman spectra of $Tb_2Ti_2O_7$ taken at 0 and 9 T with different lasers. Inset: vibrational pattern of the F_{2g} phonon (O′ ions are omitted for clarification). (b) Field evolution of the F_{2g} phonon. (c) Field dependence of the energies of $P1$ and $P2$ modes. Inset: the splitting of F_{2g} mode at low fields, collected with two polarization configurations (solid and dashed curve). (d) Polarization dependence of the $P1$ and $P2$ intensities (Raw spectra are shown in Ref. [28]).

one order of magnitude larger than that of a typical CFE at ~100 cm^{-1}; (2) the $P1$ and $P2$ energies are well below that of the CFE (~339 cm^{-1}) revealed by neutron experiments [14]; and (3) the $P2$ energy, which goes to saturation with increasing fields, exhibits a field dependence distinguished from that of a typical CFE, which normally manifests a pronounced linear field dependence.

By ruling out the above origins, we attribute the $P1$ and $P2$ modes to the splitting of the F_{2g} phonon mode, which is strongly supported by the field dependence of their energies [Fig. 1(c)] and the polarization dependence of their intensities [Fig. 1(d)]. At $H = 9$ T, the $P2$ mode locates at ~16 cm^{-1} above the $P1$ mode. The energy difference of the two modes decreases with decreasing fields and the two modes eventually merge into a single mode at ~0 T. Although it is not easy to precisely extract the $P1$ and $P2$ positions at low magnetic fields through fitting process, the polarized Raman spectra [inset of Fig. 1(c)] clearly

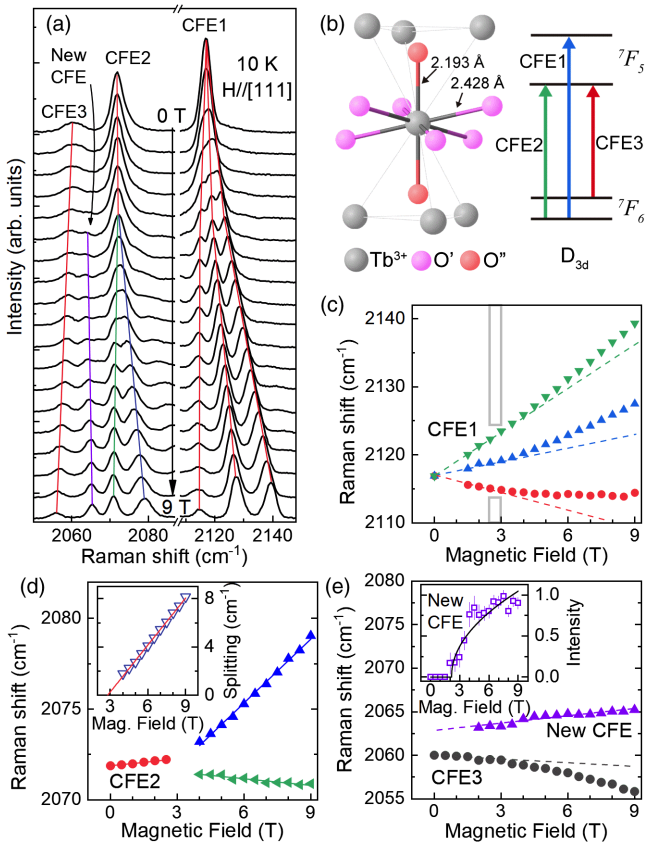

FIG. 2. Field-induced distortion of the local geometry around the Tb^{3+} ions. (a) Field evolution of the CFE spectra. (b) Local geometry around Tb^{3+} ions along with the selected crystal-field energy levels and excitations. (c),(e) Field dependence of the CFE1, CFE2, CFE3, and new CFE energies. The dashed curves are linear fits to the corresponding data. Inset of (d): energy difference of the two branches of CFE2 which goes to zero at ~3 T. Inset of (e): the integrated intensities of the new CFE. Solid curve is the fit to $I_0 + I\sqrt{H - H_c}$.

show that the energy difference between the two modes approaches to zero with decreasing fields, suggesting that the $P1$ and $P2$ modes stem from the split of the F_{2g} phonon. Moreover, the polarization dependence of the $P1$ and $P2$ intensities exhibits a clear antiphase correlation [Fig. 1(d)] indicating they share the same origin, i.e., the F_{2g} splitting. Then we conclude that the F_{2g} mode splits into two modes with the application of magnetic field along [111] axis.

The splitting of the F_{2g} mode suggests the breaking of cubic symmetries, which can be either due to a lattice modulation or a redistribution of electrons, or both. To clarify this issue, let us turn to the CFEs which directly probe the local environments around Tb^{3+} ions. Generally, magnetic fields split the CFEs and their energies are expected to linearly depend on fields due to Zeeman effects. However, if there exists a strong field-induced lattice modulation that substantially affects the crystal-field environments, the CFEs will behave anomalously, such as the nonlinear field dependence of the CFE energies, further splitting of CFEs and the emergence of new CFEs at nonzero field.

The anomalous evolutions of several CFEs under $H \parallel [111]$ are illustrated in Fig. 2(a). At zero field, three CFEs are observed at ~2117 (CFE1), 2072 (CFE2), and 2060 (CFE3) cm^{-1}. According to the crystal-field calculations [31], the three CFEs involve transitions from the $^7F_6$ manifolds to $^7F_5$ manifolds, as schematically shown in Fig. 2(b). The CFE1 splits into three strong peaks with increasing magnetic fields. The peak energies [Fig. 2(c)] exhibit nearly a linear field dependence below ~2.5 T due to the Zeeman effect, and clearly deviate from the linear behaviors at $H > 2.5$ T. The nonlinear field behaviors at $H > 2.5$ T are also witnessed by the CFE3 [Fig. 2(e)] and many other CFEs [28], systematically suggesting a change of crystal-field environments of Tb^{3+} ions.

The change of crystal-field environments is more clearly made evident by the splitting of the CFE2 and the emergence of a new CFE at ~2.5 T [Figs. 2(d) and 2(e)] which point to a distortion of the local geometry around Tb^{3+} ions. Figure 2(d) shows the field dependence of the CFE2 energies, which is linear at low fields and then splits into two peaks between 2–3 T. The CFE2 splitting starting at ~2.5 T but not 0 T [inset of Fig. 2(d)] is quite unusual and needs to be understood with the distortion of the local geometry around Tb^{3+} ions beyond the simple Zeeman effect. Meanwhile, a new CFE accompanying the CFE2 splitting appears between 2060 and 2070 cm^{-1} [Fig. 2(a)]. The normalized integrated intensities of the new CFE are shown in the inset of Fig. 2(e) and a transitionlike upturn is seen above a critical field $H_c = 2.3$ T. This demonstrates that the new CFE does not originate from the Zeeman splitting of any CFE but is related to the distortion of the local geometry around Tb^{3+} ions.

The above findings, including the F_{2g} splitting and the anomalous behaviors of CFEs under magnetic fields, allow us to conclude that a field-induced subtle structural transition occurs at H_c in $Tb_2Ti_2O_7$. Now the question is how to understand the structural transition. The low-lying first excited crystal-field state [32] and the magnetoelastic mode [23,24] seems unlikely to be the origin of the observed transition because of the small energy shift of the first excited level for $H < H_c$ (<1 cm^{-1} [28]). The fact that the observed anomalous behaviors appear only in the magnetic correlated state [28], suggests that the field-induced structural transition must be related with magnetism. Having in mind that the lattice structure of frustrated spin systems strongly depends on their magnetic structure [9,33,34] and that a field-induced magnetic transition occurs in $Tb_2Ti_2O_7$ from the zero field spin ice-liquid state to the magnetic monopole structure [3-in-1-out/3-out-1-in, Fig. 3(a)] [25], we propose that the field-induced structural transition observed in $Tb_2Ti_2O_7$ stems from the field-induced magnetic monopole structure which will be further explained below.

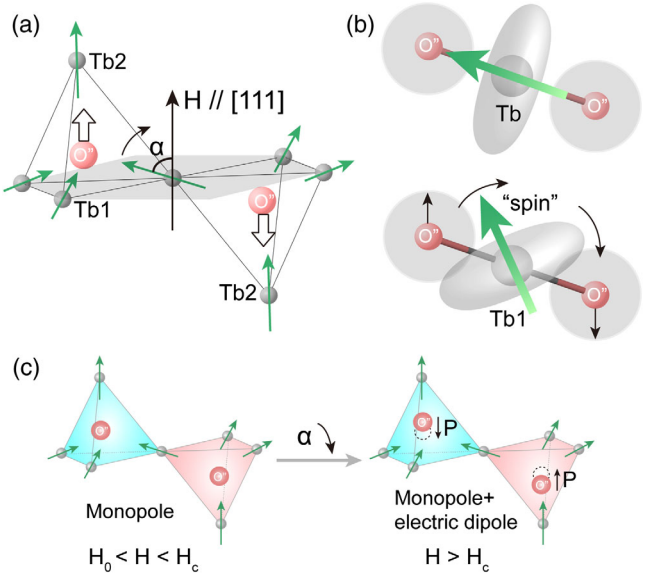

FIG. 3. Schematic illustration of magnetoelastic mechanism. (a) Electric dipoles and magnetic monopoles induced by the [111] field. Note that the displacement of O″ ions is along the [111] direction and away from the kagome plane (shaded). α is the angle between the Tb1 magnetic moments and the applied field. (b) Schematic of the oblate $4f$ charge cloud of $Tb1^{3+}$ ions (upper) and its rotation under magnetic fields (lower). (c) Field induced magnetic monopole ($H_0 < H < H_c$) and monopole plus electric dipole phase ($H > H_c$).

Unlike $3d$ ions, rare-earth ions possess a very strong spin-orbit coupling (~1 eV) which tightly locks the spin and the orbital angular momentum together, where the orbital angular momentum results from the spatially anisotropic $4f$ wave functions that can be simplicity envisioned as oblate electron charge cloud [equatorially expanded, upper of Fig. 3(b)] [35]. Because of the strong spin-orbit coupling, the orientation of the anisotropic shaped electron charge cloud is rigidly attached to the direction of the spin moment. At zero field, the system stays in the spin ice-liquid phase with magnetic moments randomly pointing into or out of tetrahedra. Meanwhile, the O″ ions reside at the center of Tb_4 tetrahedra because of the equivalence of the four O″-Tb bonds. Upon increasing field, the direction of the Tb2 moment stays parallel to the field while that of Tb1 moment continuously tilts from its original direction towards the field direction [Fig. 3(a)] [25]. Meanwhile, the strong spin-orbit coupling will drive the charge cloud ($4f$ orbit) of Tb1 ions to rotate accordingly [Fig. 3(b)] which breaks the equivalence of the four O″-Tb bonds with the O″-Tb1 bonds having much more charge clouds overlap than that of the O″-Tb2 bonds [see Fig. 3(b), Tb1: on the kagome planes; Tb2: out of kagome planes]. This will increase the Coulomb repulsion between the Tb1 and O″ ions. To minimize the overall energy, the O″ ions tend to displace away from the kagome planes along the [111] direction with the distorted phase having $R\bar{3}m$ space group (No. 166, see Ref. [28] for the distorted structure). As a result, the induced electric dipoles emerge and the system should in principle develop an antiferroelectric order [Fig. 3(c)].

The scenario well explains our experimental observations. For $H < H_c$, the Coulomb repulsion is too small to drive the displacement of O″ ions. Therefore, the field dependence of the CFEs is governed by the Zeeman effect. On the other hand, the triple F_{2g} mode vibration of O″ ions which is surrounded by Tb_4 tetrahedra [inset of Fig. 1(a)]—is very sensitive to the bonding environment of O″-Tb1 and O″-Tb2 bonds. Accompanied with the rotation of the Tb1 charge cloud, the equivalence of O″-Tb1 and O″-Tb2 bonds breaks [Fig. 3(b)] which results in the splitting of the F_{2g} mode even at $H < H_c$. For $H > H_c$, the O″-Tb1 and O″-Tb2 bonds are not further broken by the displacement of O″ ions. It explains why the $P1$ and $P2$ modes show only a kink in energy rather than a jump when crossing the transition. However, the real displacement of O″ ions changes the local geometry of Tb^{3+} ions, resulting in the observed anomalous behaviors of CFEs. The peak bifurcation of CFE2 above H_c is a natural consequence of the inequivalence of crystal-field environments between Tb1 (C_1 site symmetry) and Tb2 (D_{3d} site symmetry) [28]. And the variations of CF wave functions caused by the displacement in principle relax the CF transition rules and render some transitions visible in Raman channel, i.e., the emergence of the new CFE peak.

To confirm the formation of electric dipoles, we turn to the magnetodielectric response of this material. As shown in Figs. 4(a) and 4(b), the low-temperature dielectric permittivity ε exhibits a pronounced rise with increasing field and its slope reaches maximum value at around 2–3 T, consistent with our Raman observations. The enhancement

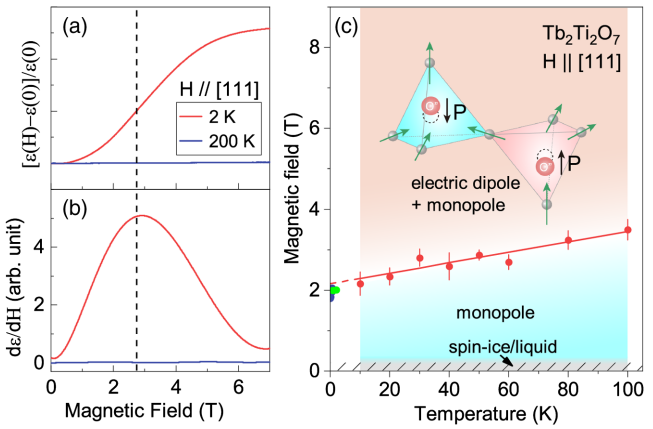

FIG. 4. Field dependence of (a) dielectric permittivity ε and (b) $d\varepsilon/dH$ at 2 and 200 K. (c) [111] field vs temperature phase diagram of $Tb_2Ti_2O_7$. The raw data can be found in Ref. [28] and the critical fields are determined by the similar analysis to Fig. 2(e). The solid blue and green circles are the H_2/H_s values taken from Refs. [36] and [37], respectively.

of ε strongly suggests the emergence of extra electric dipoles with increasing magnetic field. In contrast, ε is nearly constant with magnetic field at high temperatures. These results further support our proposal that the induced electric dipoles are related to the magnetic monopole structures at low temperatures, thus, they should strongly couple with each other. Based on the above, we conclude that the concurrence of monopoles and coupled electric dipoles is realized in $Tb_2Ti_2O_7$.

By carrying out field-dependent Raman measurements and analysis similar to Fig. 2(e) for different temperatures, we tracked the temperature dependence of H_c [see Fig. 4(c)]. From 10 to 100 K, H_c linearly increases from ~2.3 to 3.5 T [see Fig. 4(c)]. Interestingly, the extrapolated field at zero temperature (~2.1 T) agrees well with the field H_2 given by susceptibility [36] and H_s by thermal conductivity [37]. It suggests that the transition at H_2/H_s reported by thermodynamic measurements, is related to the structural transition observed here. The finding may be a key to understanding the anomalous thermal conductivity observed in $Tb_2Ti_2O_7$ [37].

Let us conclude the Letter by discussing the key consequence of the field induced structural transition in $Tb_2Ti_2O_7$, the emergence of electric dipole on its magnetic monopole. $Tb_2Ti_2O_7$ is thus a promising candidate in which the magnetic "monopoles" have both magnetic charges and coupled electric dipoles. The study makes the close analogy of electricity and magnetism go even further than usually assumed, i.e., the counterpart of a point charge (electron) not allowed in the fundamental level, can be realized as an emergent particle in condensed matter systems. This may bring many new and intriguing possibilities and greatly extend the study of pyrochlore spin systems. For example, the coupling between magnetic monopoles and electric dipoles allows us to study and control the monopoles by external electric fields, i.e., creation, elimination, and separation of monopoles and antimonopoles.

This work was supported by the Ministry of Science and Technology of China (No. 2017YFA0302904 and No. 2016YFA0300504) and the NSF of China (No. 11774419 and No. 11474357). X. Q. W. is supported by MOST: 2016YFA0300501 and NSFC: 11974244 and additionally from a Shanghai talent program.

F. J. and C.-L. L. contributed equally to this work.

*qmzhang@ruc.edu.cn

[1] M. Fiebig, T. Lottermoser, D. Meier, and M. Trassin, Nat. Rev. Mater. **1**, 16046 (2016).
[2] S.-W. Cheong and M. Mostovoy, Nat. Mater. **6**, 13 (2007).
[3] D. Khomskii, Physics **2**, 20 (2009).
[4] D. Khomskii, Nat. Commun. **3**, 904 (2012).
[5] D. I. Khomskii, J. Phys. Condens. Matter **22**, 164209 (2010).
[6] C. P. Grams, M. Valldor, M. Garst, and J. Hemberger, Nat. Commun. **5**, 4853 (2014).
[7] M. J. P. Gingras, Science **326**, 375 (2009).
[8] J. S. Gardner, M. J. P. Gingras, and J. E. Greedan, Rev. Mod. Phys. **82**, 53 (2010).
[9] B. Stojanovic, *Magnetic, Ferroelectric, and Multiferroic Metal Oxides* (Cambridge University Press, Cambridge, England, 2018).
[10] S. Dong, J.-M. Liu, S.-W. Cheong, and Z. Ren, Adv. Phys. **64**, 519 (2015).
[11] L. D. C. Jaubert and R. Moessner, Phys. Rev. B **91**, 214422 (2015).
[12] M. J. P. Gingras, B. C. den Hertog, M. Faucher, J. S. Gardner, S. R. Dunsiger, L. J. Chang, B. D. Gaulin, N. P. Raju, and J. E. Greedan, Phys. Rev. B **62**, 6496 (2000).
[13] A. J. Princep, H. C. Walker, D. T. Adroja, D. Prabhakaran, and A. T. Boothroyd, Phys. Rev. B **91**, 224430 (2015).
[14] M. Ruminy, E. Pomjakushina, K. Iida, K. Kamazawa, D. T. Adroja, U. Stuhr, and T. Fennell, Phys. Rev. B **94**, 024430 (2016).
[15] J. S. Gardner, S. R. Dunsiger, B. D. Gaulin, M. J. P. Gingras, J. E. Greedan, R. F. Kiefl, M. D. Lumsden, W. A. MacFarlane, N. P. Raju, J. E. Sonier, I. Swainson, and Z. Tun, Phys. Rev. Lett. **82**, 1012 (1999).
[16] K. Fritsch, K. A. Ross, Y. Qiu, J. R. D. Copley, T. Guidi, R. I. Bewley, H. A. Dabkowska, and B. D. Gaulin, Phys. Rev. B **87**, 094410 (2013).
[17] T. Fennell, M. Kenzelmann, B. Roessli, M. K. Haas, and R. J. Cava, Phys. Rev. Lett. **109**, 017201 (2012).
[18] S. Petit, P. Bonville, J. Robert, C. Decorse, and I. Mirebeau, Phys. Rev. B **86**, 174403 (2012).
[19] S. Guitteny, J. Robert, P. Bonville, J. Ollivier, C. Decorse, P. Steffens, M. Boehm, H. Mutka, I. Mirebeau, and S. Petit, Phys. Rev. Lett. **111**, 087201 (2013).
[20] I. V. Aleksandrov, B. V. Lidsky, L. G. Mamsurova, M. G. Neigauz, K. S. Pigalskii, K. K. Pukhov, N. G. Trusevich, and L. G. Shcherbakova, Sov. Phys. J. Exp. Theor. Phys. **62**, 1287 (1985).
[21] L. G. Mamsurova, K. S. Pigalskii, and K. K. Pukhov, J. Exp. Theor. Phys. Lett. **43**, 755 (1986).
[22] J. P. C. Ruff, Z. Islam, J. P. Clancy, K. A. Ross, H. Nojiri, Y. H. Matsuda, H. A. Dabkowska, A. D. Dabkowski, and B. D. Gaulin, Phys. Rev. Lett. **105**, 077203 (2010).
[23] T. Fennell, M. Kenzelmann, B. Roessli, H. Mutka, J. Ollivier, M. Ruminy, U. Stuhr, O. Zaharko, L. Bovo, A. Cervellino, M. K. Haas, and R. J. Cava, Phys. Rev. Lett. **112**, 017203 (2014).
[24] M. Ruminy, S. Guitteny, J. Robert, L.-P. Regnault, M. Boehm, P. Steffens, H. Mutka, J. Ollivier, U. Stuhr, J. S. White, B. Roessli, L. Bovo, C. Decorse, M. K. Haas, R. J. Cava, I. Mirebeau, M. Kenzelmann, S. Petit, and T. Fennell, Phys. Rev. B **99**, 224431 (2019).
[25] A. P. Sazonov, A. Gukasov, H. B. Cao, P. Bonville, E. Ressouche, C. Decorse, and I. Mirebeau, Phys. Rev. B **88**, 184428 (2013).
[26] A. P. Sazonov, A. Gukasov, I. Mirebeau, and P. Bonville, Phys. Rev. B **85**, 214420 (2012).
[27] Q. Li, L. Xu, C. Fan, F. Zhang, Y. Lv, B. Ni, Z. Zhao, and X. Sun, J. Cryst. Growth **377**, 96 (2013).

[28] See Supplemental Material at http://link.aps.org/supplemental/10.1103/PhysRevLett.124.087601 for details on the characterization of the used sample and the temperature dependence of the observed anomalous behaviors.
[29] T. T. A. Lummen, I. P. Handayani, M. C. Donker, D. Fausti, G. Dhalenne, P. Berthet, A. Revcolevschi, and P. H. M. van Loosdrecht, Phys. Rev. B **77**, 214310 (2008).
[30] V. A. Chernyshev, V. P. Petrov, and A. E. Nikiforov, Phys. Solid State **57**, 996 (2015).
[31] V. V. Klekovkina and B. Z. Malkin, Opt. Spectrosc. **116**, 849 (2014).
[32] H. R. Molavian, M. J. P. Gingras, and B. Canals, Phys. Rev. Lett. **98**, 157204 (2007).
[33] T. Kimura, T. Goto, H. Shintani, K. Ishizaka, T. Arima, and Y. Tokura, Nature (London) **426**, 55 (2003).
[34] H. C. Walker, F. Fabrizi, L. Paolasini, F. de Bergevin, J. Herrero-Martin, A. T. Boothroyd, D. Prabhakaran, and D. F. McMorrow, Science **333**, 1273 (2011).
[35] G. Engdahl, *Handbook of Giant Magnetostrictive Materials* (Academic Press, New York, 2000).
[36] S. Legl, C. Krey, S. R. Dunsiger, H. A. Dabkowska, J. A. Rodriguez, G. M. Luke, and C. Pfleiderer, Phys. Rev. Lett. **109**, 047201 (2012).
[37] M. Hirschberger, J. W. Krizan, R. J. Cava, and N. P. Ong, Science **348**, 106 (2015).